Analysis of gradient elution chromatography using the transport model

Shamsul Qamar[a,b], Nazia Rehman[a], Giorgio Carta[c], Andreas Seidel-Morgenstern[b]

[a]*Department of Mathematics, COMSATS University Islamabad, Pakistan*
[b]*Max Planck Institute for Dynamics of Complex Technical Systems, Magdeburg, Germany*
[c]*Department of Chemical Engineering, University of Virginia, Charlottesville, Virginia, USA*

Abstract

A transport model is considered to describe gradient elution in liquid chromatography in packed beds with the linear isotherm dependent on the mobile phase modulator. By applying a coordinate transformation, the model is solved analytically using the Laplace transform approach. The moment generating property of the Laplace domain solution is used to derive analytical expressions for the first three moments of the response to rectangular injections. These moments are instructive for analyzing the retention time, band broadening and asymmetry of elution profiles. Compared to isocratic elution, the derivation of analytical solutions and moments for gradient elution is more complicated, because the retention behavior of the solutes depends on the varying mobile phase modulator. Several case studies are evaluated theoretically. To gain confidence on the derived analytical results, a high-resolution finite volume scheme is also applied to solve the same model equations numerically. The analytical solutions and moments provided are utilized to predict the effects of starting and ending times of gradient, magnitude of modulator con-

*Corresponding author. Tel: +49-391-6110454; fax: +49-391-6110500
Email addresses: qamar@mpi-magdeburg.mpg.de (Shamsul Qamar)

centration variation, gradient slopes, and mass transfer coefficient on retention and peak shape. The analytical moment expressions derived can be used to determine retention and mass transfer parameters from experimental peaks and to predict elution behaviors if these parameters are known.
Key words: Liquid chromatography, gradient elution, transport model, coordinate transformation, analytical solutions, moment analysis.

1. Introduction

Gradient elution chromatography is a well-known chromatographic technique that can improve the separation of complex mixtures containing components of widely different elution behavior, see Jandera et al. (1985); Snyder (1986); Snyder and Dolan (1998); Jandera (2005). Since its introduction in the early 1950s, it is used extensively for analytical and preparative applications, see Jandera (2005); Hagdahl et al. (1952); Donaldson et al. (1952). The technique improves considerably the peak detection capabilities in liquid chromatography (e.g. Hoe et al. (2006, 2013); Carta and Stringfield (1992)). Additionally, it provides a more robust operation compared to isocratic elution when retention is a very strong function of the mobile phase modifier, as in the case of the chromatography of proteins and other macromolecules. Gradient elution chromatography is based on the programmed change in mobile-phase composition and/or column temperature. In liquid chromatography, the change in the mobile phase composition is the widely used option. After injecting a sample into the column, the concentration of a suitable mobile phase modulator (ϕ) can be changed in order to alter specifically the interaction strength of the sample components

with the stationary phase (see e.g. Donaldson et al. (1952)). Typically, the change in the ϕ is gradual but can also be stepwise or in a series of steps. Compared to isocratic elution, the theoretical analysis of gradient elution is more complicated. Theoretical and practical aspects of gradient elution chromatography are summarized in the books of Jandera et al. (1985) and Snyder and Dolan (2006) and in the review paper of Jandera (2006). Concepts to predict retention times during gradient elution are described by Baeza-Baeza et al. (2013).

Most important for quantifying migration processes under the influence of solvent gradients is knowledge of the relation between modulator concentrations and the component specific adsorption equilibrium constants. The linear solvent strength (LSS) model is widely used to describe this relationship (see e.g. Snyder (1986); Carta and Stringfield (1992); Carta et al. (2018); Hoe et al. (2006, 2013); Ståhlberg (2010)). The LSS model assumes that the Henry constant (k_H) varies exponentially with the mobile phase composition in reversed phase chromatography (RPC), according to the following equation:

$$k_H(\phi) = k_{H_r} e^{-\alpha\phi}, \tag{1}$$

where k_{H_r} is the component-specific reference Henry constant (at $\phi = 0$) and α is a component-specific parameter that quantifies the sensitivity of the Henry constant to changes in ϕ.

The equilibrium dispersive (ED) and transport (TR) models are frequently used to describe the dynamics of band profiles in liquid chromatography, see Nicoud (2015); Guiochon (2002); Miyabe and Guiochon (2000); Guan-Sajonz et al. (1996). In the ED model, all the

contributions to band broadening are lumped into an apparent axial dispersion coefficient (D_a). Alternatively, the TR model describes band brodening using a mass transfer rate model based on a single mass transfer coefficient k_m with a linear driving force expressed by the difference between the equilibrium and the actual adsorbed phase concentrations of the solute in the stationary phase. The mass transfer coefficient k_m lumps together the two contributions of internal and external mass transfer resistances.

In this work, we use the TR model assuming that the rate coefficient does not depend on ϕ. An appropriate coordinate transformation and the Laplace transform approach are jointly applied to solve the TR model analytically in the Laplace domain, see Javeed et al. (2013). Because of the complexity of the solution, a time domain solution can be obtained by using an efficient and accurate numerical Laplace inversion technique such as that of Durbin (1974). Thus, the moment generating property of the Laplace domain solution is exploited to derive analytical expressions for the first three analytical moments. These moments are useful for analyzing and interpreting measured elution profiles and to predict peak retention, breadth, and skewness. In the literature, moment analysis is known to be a very effective strategy for deducing important information about the equilibrium and mass transfer in the column, see Schneider and Smith (1968); Kucera (1965); Suzuki (1973); Guiochon et al. (2006); Miyabe et al. (2007, 2009). To get confidence in the correctness of the derived analytical results, a high-resolution finite volume scheme (HR-FVS) is applied in parallel to solve the model equations numerically (see e.g. Javeed et al. (2011)). The effects of starting and ending times of gradient, the magnitude of altering the modulator concentration, gradient slopes, and mass transfer coefficient are analyzed on the elution

profiles and moments.

This article is arranged as follows. In Section 2, the transport model is formulated for gradient elution liquid chromatography in a fixed-bed column. In Section 3, suitable new variables are introduced that support deriving the solutions. In Section 4, the Laplace transform approach is applied to solve the model equations analytically. In Section 5, the relevant time domain moments are obtained. Section 6 presents results of several case studies. Finally, conclusions are presented in Section 7.

2. The mathematical model

In this study, the TR model is considered for gradient elution lumping together all contributions to band broadening into one rate constant. Further, it is assumed that this constant k_m is independent of ϕ. The conservation equations for the solute in the two phases are given by

$$\frac{\partial c}{\partial t} + F\frac{\partial q}{\partial t} + u\frac{\partial c}{\partial z} = 0, \tag{2}$$

$$\frac{\partial q}{\partial t} = k_m(q^*(\phi(t,z)) - q), \tag{3}$$

where c is the concentration of solute in the liquid phase, q is the actual solute concentration in the solid phase, q^* is the equilibrium solute concentration in the solid phase, u is the interstitial velocity, $F = (1-\epsilon)/\epsilon$ is the phase ratio with ϵ being the external porosity, t is time and z is the axial-coordinate.

The initial conditions for an initially fully regenerated column are:

$$c(0,z) = 0, \quad q(0,z) = 0. \tag{4}$$

An appropriate inlet boundary condition is required for Eq. (2). In this study, we consider rectangular pulse injections described by a Dirichlet boundary condition:

$$c(t,0) = \begin{cases} c_{\text{inj}}\,, & \text{if } 0 \le t \le t_{\text{inj}}\,, \\ 0\,, & t > t_{\text{inj}}. \end{cases} \tag{5}$$

Here, c_{inj} denotes the injected concentration and t_{inj} is the time of injection.

The concentration of the varying mobile phase modulator, $\phi(t,z)$, at any time and at any position inside the column determines the local migration speed of the solute. The modulator is assumed to be unretained and its profile within the column is assumed to be unaffected by band broadening. This is a somewhat restrictive assumption, which needs to be checked when applying the model analyzed in this paper. As a result, we can use the ideal model to describe the ϕ as a function of time and distance in the column. The ideal model accounting for change in the concentration of the modulator in the mobile phase can be written for a column of length L as

$$\frac{\partial \phi}{\partial t} + u\frac{\partial \phi}{\partial z} = 0, \tag{6}$$

$$\phi(0,z) = \phi_0, \quad 0 \le z \le L, \tag{7}$$

$$\phi(t,0) = \begin{cases} \phi_0\,, & \text{if } t < t_s, \\ \Phi(t - t_s)\,, & \text{if } t_s \le t \le t_{\text{e}}, \\ \phi_e\,, & t > t_{\text{e}}, \end{cases} \tag{8}$$

where, t_s and t_e denote the starting and ending times of the gradient. Further, ϕ_0 denotes the initial concentration of the modulator, Φ is the implemented gradient profile which

can be of arbitrary shape and ϕ_e is the final concentration of the modulator in the solvent reached at time t_e (the time at which gradient ends) and is kept constant afterwards.

For a linear gradient holds

$$\Phi(t) = \phi_0 + \tilde{\beta} t \,, \tag{9}$$

where

$$\tilde{\beta} = (\phi_e - \phi_0)/(t_e - t_s), \tag{10}$$

is the slope (or steepness) of the gradient. Furthermore, if the adsorption equilibrium is assumed to be linear $\phi \in [\phi_0, \phi_e]$, we have

$$q^*(t, z) = k_H(\phi(t, z))c(t, z). \tag{11}$$

In this work, we assume that the Henry's constant k_H depends exponentially on the modulator concentration ϕ as given in Eq. (1) (LSS-model).

3. Introduction of new variables

Let us define the two new variables

$$\eta = \frac{t}{t_0}, \quad \xi = \frac{t}{t_0} - \frac{z}{L}, \tag{12}$$

where, $t_0 = L/u$ is the retention time of a non-retained component ($k_H = 0$) and ξ represents an implementation of a "moving observer". Application of the chain rule gives

for the relevant derivatives:

$$\frac{\partial c}{\partial t} = \frac{\partial c}{\partial \eta}\frac{d\eta}{dt} + \frac{\partial c}{\partial \xi}\frac{d\xi}{dt} = \frac{1}{t_0}\left[\frac{\partial c}{\partial \eta} + \frac{\partial c}{\partial \xi}\right], \tag{13}$$

$$\frac{\partial q}{\partial t} = \frac{\partial q}{\partial \eta}\frac{d\eta}{dt} + \frac{\partial q}{\partial \xi}\frac{d\xi}{dt} = \frac{1}{t_0}\left[\frac{\partial q}{\partial \eta} + \frac{\partial q}{\partial \xi}\right], \tag{14}$$

$$\frac{\partial c}{\partial z} = \frac{\partial c}{\partial \eta}\frac{d\eta}{dz} + \frac{\partial c}{\partial \xi}\frac{d\xi}{dz} = -\frac{1}{L}\frac{\partial c}{\partial \xi} = -\frac{1}{ut_0}\frac{\partial c}{\partial \xi}. \tag{15}$$

Accordingly, the balance equations, Eqs. (2) and (3), reduce to:

$$\frac{\partial (c + Fq)}{\partial \eta} + F\frac{\partial q}{\partial \xi} = 0, \tag{16}$$

$$\frac{\partial q}{\partial \eta} + \frac{\partial q}{\partial \xi} = \kappa_m (k_H(\xi)c - q), \tag{17}$$

where $\kappa_m = t_0 k_m$ and $k_H(\xi) = k_H(\phi(\xi))$. Further, $\phi(\xi)$ is obtained by solving Eq. (6) for the given initial and boundary conditions (c.f. Eqs. (7) and (8)):

$$\phi(\xi) = \begin{cases} \phi_0\,, & \text{if } \xi < \eta_s\,, \\ \Phi(\xi - \eta_s)\,, & \text{if } \eta_s \le \xi \le \eta_e\,, \\ \phi_e\,, & \xi > \eta_e, \end{cases} \tag{18}$$

where $\eta_s = t_s/t_0$, $\eta_e = t_e/t_0$, $\Phi(\xi) = \phi_0 + \beta\xi$, and

$$\beta = (\phi_e - \phi_0)/(\eta_e - \eta_s). \tag{19}$$

Ahead of the advancing solution, specified by $t = z/u$, i.e. for $\xi = 0$ and $t \ge 0$, the solute concentration cannot exceed zero, because the solute is retained by the stationary phase and dispersion is neglected in the transport model. Therefore, the initial conditions become:

$$c(\eta = 0, \xi) = 0, \quad q(\eta = 0, \xi) = 0, \text{ for } \xi \ge 0. \tag{20}$$

For the rectangular pulse injections considered, the BC (Eq. (5)) is modified into

$$c(\eta,0)=\begin{cases} c_{\text{inj}}\,, & \text{if } 0<\eta\leq\eta_{\text{inj}}\,,\\ 0\,, & \eta>\eta_{\text{inj}}. \end{cases} \tag{21}$$

Here, $\eta_{\text{inj}}=t_{\text{inj}}/t_0$.

4. Analytical solution of the model in the Laplace domain

Next, we apply the Laplace transformation to solve the model equations. The Laplace transformed c and q with respect to η are given as (see e.g. Nicoud (2015))

$$\bar{c}(s,\xi)=\int_0^\infty e^{-s\eta}c(\eta,\xi)d\eta,\quad \bar{q}(s,\xi)=\int_0^\infty e^{-s\eta}q(\eta,\xi)d\eta. \tag{22}$$

By applying the Laplace transformation on Eq. (17), we obtain the following ODE

$$\bar{c}(s,\xi)=\frac{1}{\kappa_m k_H(\xi)}\left[(s+\kappa_m)\bar{q}(s,\xi)+\frac{d\bar{q}(s,\xi)}{d\xi}\right]. \tag{23}$$

Similarly, Eq. (16) gives

$$s[\bar{c}(s,\xi)+F\bar{q}(s,\xi)]+F\frac{d\bar{q}(s,\xi)}{d\xi}=0. \tag{24}$$

On using Eq. (23) in Eq. (24), we obtain

$$\frac{d\bar{q}(s,\xi)}{d\xi}+s\left(1+\frac{\kappa_m}{s+Fk_H(\xi)\kappa_m}\right)\bar{q}(s,\xi)=0. \tag{25}$$

The solution of the above equation is given by

$$\bar{q}(s,\xi)=A\exp\left(-s\xi-\int_0^\xi\frac{s\kappa_m}{s+Fk_H(\theta)\kappa_m}d\theta\right). \tag{26}$$

The next step is to specify the constant A. We already know the boundary condition for the liquid phase concentration $\bar{c}(s,0)$ but not for the solid phase concentration $\bar{q}(s,0)$. The Laplace transformation of Eq. (17) at $\xi = 0$ gives

$$s\bar{q}(s,0) + \left.\frac{\partial \bar{q}(s,\xi)}{\partial \xi}\right|_{\xi=0} = \kappa_m[k_H(\phi_0)\bar{c}(s,0) - \bar{q}(s,0)]. \tag{27}$$

For a rectangular pulse injection (c.f. Eq. (21)), the Eqs. (26) and (27) give

$$A = c_{\text{inj}}\left[\frac{s + Fk_H(\phi_0)\kappa_m}{F\kappa_m}\right]\left[\frac{1 - e^{-s\eta_{\text{inj}}}}{s}\right]. \tag{28}$$

Using the above values of A in Eq. (26) we obtain $\bar{q}(s,\xi)$ which is then used along with its derivative in Eq. (23) to obtain $\bar{c}(s,\xi)$. Thus, the concentration in the bulk phase can be expressed in the Laplace domain as

$$\bar{c}(s,\xi) = c_{\text{inj}}\left[\frac{s + Fk_H(\phi_0)\kappa_m}{s + Fk_H(\xi)\kappa_m}\right]\left[\frac{1 - e^{-s\eta_{\text{inj}}}}{s}\right]\exp\left(-s\xi - \kappa_m\int_0^{\xi}\frac{s}{s + Fk_H(\theta)\kappa_m}d\theta\right), \text{ for } \xi \geq 0. \tag{29}$$

According to Eq. (18), we obtain

$$k_H(\xi) = \begin{cases} k_H(\phi_0), & \text{for } 0 \leq \xi < \eta_s, \\ k_H(\Phi(\xi - \eta_s)), & \text{for } \eta_s \leq \xi \leq \eta_e, \\ k_H(\phi_e), & \text{for } \xi > \eta_e. \end{cases} \tag{30}$$

Here, $\Phi(\xi - \eta_s) = \phi_0 + \beta(\xi - \eta_s)$, $\beta = (\phi_e - \phi_0)/(\eta_e - \eta_s)$ and $k_H(\phi)$ is given by in by Eq. (1) for $\phi \in \{\phi_0, \Phi, \phi_e\}$.

4.1. Analytical solution in the (s,x) coordinates

One can find a relation between (s,x) coordinates and (s,ξ) coordinates in the Laplace domain by using Eqs. (2), (3), (16) and (17) in the ξ-domain. After some simple manipu-

lations, we obtain:

$$\frac{dx}{d\xi} = \frac{se^{-\alpha\beta(\tilde{\xi}-\eta_s)} + \kappa_m}{s + Fk_H(\theta)\kappa_m}, \quad \text{for } \tilde{\xi} \in (\eta_s, \eta_e), \tag{31}$$

or

$$\int_0^{\xi} \frac{1}{s + Fk_H(\theta)\kappa_m} d\theta = \frac{x}{se^{-\alpha\beta(\tilde{\xi}-\eta_s)} + \kappa_m}. \tag{32}$$

By using the above transformation, the ξ-domain solution in Eq. (29) is converted into the x-domain solution as

$$\bar{c}(s,x) = c_{\text{inj}} \left[\frac{1 - e^{-s\eta_{\text{inj}}}}{s}\right] \exp\left(-sf(s,x) - \frac{\kappa_m x}{se^{-\alpha\beta(\tilde{\xi}-\eta_s)} + \kappa_m}\right), \tag{33}$$

where, due to Eq. (32), $f(s,x) := \xi(s,x)$ is given as

$$f(s,x) = \begin{cases} \frac{s+Fk_H(\phi_0)\kappa_m}{s+\kappa_m} x, \quad 0 \le \xi < \eta_s, \\ \eta_s + \frac{1}{\alpha\beta} \ln[\frac{(s+Fk_H(\phi_0)\kappa_m)}{s} e^{s\alpha\beta\left(\frac{x}{s+\kappa_m} - \frac{\eta_s}{s+Fk_H(\phi_0)\kappa_m}\right)} - \frac{Fk_H(\phi_0)\kappa_m}{s}], \ \eta_s \le \xi \le \eta_e, \\ \eta_e + [s + Fk_H(\phi_e)\kappa_m]\left[\frac{x}{s+\kappa_m} - \frac{\eta_s}{s+Fk_H(\phi_0)\kappa_m} - \frac{1}{s\alpha\beta} \ln[\frac{se^{\alpha\beta(\eta_e-\eta_s)} + Fk_H(\phi_0)\kappa_m}{s+Fk_H(\phi_0)\kappa_m}]\right], \ \xi > \eta_e. \end{cases} \tag{34}$$

Eqs. (33) and (34) are inverted numerically to get the time domain solution. As $\tilde{\xi} \in (\eta_s, \eta_e)$, we can choose any value of $\tilde{\xi}$ between η_s and η_e. In our numerical computations, we have chosen $\tilde{\xi} = (3\eta_s + 2\eta_e)/5$ which gives better agreement with the numerical results of HR-FVS.

5. Analytical moments

The analytical expressions of temporal moments in the (η, ξ) and (η, x) coordinates are derived in Appendix A, while these moments in (t, z) coordinates are given below.

The area of the eluted peak is given by (c.f.(A-14))

$$\mu_0 = c_{\text{inj}} t_{\text{inj}}. \tag{35}$$

The mean retention time is given by (c.f.(A-15))

$$\mu_1 = \frac{t_{\rm inj}}{2} + t_0(1+\xi_R) - \frac{1}{k_m}\left[\frac{1}{Fk_H(\phi_0)} - \frac{1}{Fk_H(\xi_R)}\right]. \tag{36}$$

The breadth of the peak is described by the second central moment which is given by (c.f.(A-18))

$$\mu_2' = \frac{t_{\rm inj}^2}{12} + \frac{2t_0F^2k_H^2(\tilde{\xi}_R)}{k_m}\int_0^{\xi_R}\frac{1}{F^2k_H^2(\theta)}d\theta - \frac{1}{k_m^2}\left[\frac{F^2k_H^2(\tilde{\xi}_R)}{F^2{k_H}^2(\phi_0)} - \frac{F^2k_H^2(\tilde{\xi}_R)}{F^2k_H^2(\xi_R)}\right]. \tag{37}$$

Here, $\tilde{\xi}_R \in (\xi_R, \xi_0)$, $\xi_0 = Fk_H(\phi_0)$ and ξ_R is given by Eq. (A-4) of the Appendix A. Finally, the skewness of the peak is described by the third central moment which is given by (c.f.(A-19))

$$\mu_3' = \frac{6t_0F^3k_H^3(\tilde{\xi}_R)}{k_m^2}\int_0^{\xi_R}\frac{1}{F^3k_H^3(\theta)}d\theta - \frac{2}{k_m^3}\left[\frac{F^3k_H^3(\tilde{\xi}_R)}{F^3k_H^3(\phi_0)} - \frac{F^3k_H^3(\tilde{\xi}_R)}{F^3k_H^3(\xi_R)}\right]. \tag{38}$$

The analytical solutions of the integrals in the second and third central moments are given by Eq. (A-13) of the Appendix A. As $\tilde{\xi}_R \in (\xi_R, \xi_0)$, we can choose any value of $\tilde{\xi}_R$ between ξ_R and ξ_0. In our numerical computations, we have chosen the value of $\tilde{\xi}_R = 1.04\xi_R$ which gives better agreement with the numerical moments.

5.1. Limiting case for isocratic elution

For isocratic elution ($\beta = 0$), the above moments (c.f. Eqs.(35), (36), (37) and (38)) reduce to:

$$\mu_{0,\mathrm{iso}} = c_{\mathrm{inj}} t_{\mathrm{inj}}, \tag{39}$$

$$\mu_{1,\mathrm{iso}} = \frac{t_{\mathrm{inj}}}{2} + t_0[1 + F k_H(\phi_0)], \tag{40}$$

$$\mu'_{2,\mathrm{iso}} = \frac{t_{\mathrm{inj}}^2}{12} + \frac{2 t_0 F k_H(\phi_0)}{k_m}, \tag{41}$$

$$\mu'_{3,\mathrm{iso}} = \frac{6 t_0 F k_H(\phi_0)}{k_m^2}. \tag{42}$$

These expressions agree with the well-known relationships already available in the literature (see e.g. Javeed et al. (2013)). These moment expressions can be used to calculate directly other commonly used peak properties, such as HETP= $L\mu'_2/\mu_1^2$.

6. Numerical case studies

In this section, various case studies are provided to illustrate selected elution profiles and corresponding moments obtained from the semi-analytical solution (c.f. Eq. (33)) and from the analytical expressions for the temporal moments (c.f. Eqs. (35)-(38)). In the figures, the solute concentration (c) and the modulator concentration (ϕ) are plotted over time (t) at the column outlet ($z = L$). Furthermore, temporal moments are plotted with respect to different operational parameters appearing in the model equations. The reference parameters used in the case studies are listed in Table 1. These model parameters are chosen in accordance with ranges common in liquid chromatography applications.

6.1. Effects of different parameters on elution profiles and moments

Figure 1(a) compares the first elution profiles for two isocratic cases ($\beta = 0$ and $\phi(\xi) = \phi_0$ or $\phi(\xi) = \phi_e$) with the profile obtained for elution with a linear gradient ($\beta \neq 0$ and $\phi(\xi)$ according to Eq. (18)). As expected, it can be seen that isocratic elution with $\phi(\xi) = \phi_0$ produces a wider profile with a longer retention time and larger variance and asymmetry ($\mu_1 = 80.1$ min, $\mu_2' = 14.2$ min^2 and $\mu_3' = 4.2$ min^3). On the other hand, isocratic elution with $\phi(\xi) = \phi_e$ produces a comparatively narrow and more symmetric earlier eluting profile ($\mu_1 = 57.45$ min, $\mu_2' = 9.64$ min^2 and $\mu_3' = 2.79$ min^3). Lastly, gradient elution generates a profile which is most symmetric and narrow lying between the two isocratic cases ($\mu_1 = 71.24$ min, $\mu_2' = 9.1$ min^2 and $\mu_3' = 2.32$ min^3). Figure 1(b) gives the elution profiles for different gradient steepnesses obtained by changing ϕ_e (or β/t_0 in Eq. (19)), while all other parameters are taken from Table 1. The well-known acceleration effect of steeper gradients is correctly captured by the solution. A comparison of semi-analytical solutions for concentration (shown by lines in Figure 1(a)&(b)) with the numerical solutions of high-resolution finite volume scheme (HR-FVS) (shown by symbols in Figure 1(a)&(b)) verifies the correctness of our semi-analytical solutions.

Figures 2 and 3 illustrate the impact of altering the ending and starting times of the gradients individually for a fixed gradient steepness and magnitude.

Figure 2 displays the effect of gradient ending time (t_e) for a fixed starting time of $t_s = 5$ min on the elution profiles and moments. One limiting case arises if $t_e = t_s = 5$ min, which describes a situation, where after this short delay there is an immediate switch to the isocratic situation with $\phi = 0.6$. This delay makes the first and third moments

slightly smaller and the second moment slightly larger compared to the fully isocratic case discussed in Figure 1. Increasing the ending time, i.e. introducing shallower gradients, slows down the chromatograms and makes the peaks more narrower and more symmetric. However, this trend stops if the gradients are so shallow that the elution is controlled by the initial elution strength. Then the corresponding limits of the moments given in Figure 1 are asymptotically reached. In the particular example illustrated the turning point is approximately at $t_e = 55$ min.

Figure 3 displays the effect of modulator starting time (t_s) for a fixed ending time of 80 min on the elution profiles and moments. Similar behavior as shown in Figure 2 can be seen in the limiting cases of very shallow and very fast gradients. The elution profiles and also the corresponding three moments approach the limiting situations for the isocratic cases illustrated in Figure 1. Again a transition region can be seen where the second and third moments are smaller than in the two limiting situations (in the example for t_s between 30 and 40 min).

Figure 4 shows the effect of solvent strength parameter (α) on the elution profiles and moments. It can be seen that profiles become narrower and more symmetric with reduced retention time when α is increased from 0.001 to 4, i.e. when the sensitivity of the Henry constant with respect to the modulator concentration is increased.

Figure 5 displays the effects of the mass transfer coefficient (k_m) on the elution profiles and moments. It can be seen that the profiles become narrower and symmetric when k_m is increased from 1 min^{-1} to 50 min^{-1}. However, as expected, the mean retention time is not affected by k_m.

As in Figure 2, to show the flexibility of the solution space covered, Figure 6 displays but now the effect of gradient ending time (t_e) for the case of negative gradient (i.e. $\phi_e < \phi_0$) on the elution profiles and moments. The results predicted by our solution are consistent with the expected behavior, including the fact that there exists now a distinct gradient ending time t_e for which the second and third moments have maxima (approx. for 55 min).

6.2. Peak compression factor

The most comprehensive treatment of gradient elution chromatography is based on the linear solvent strength (LSS) theory of Snyder (1986); Snyder and Dolan (2006). This theory has been developed for infinitesimal feed pulses. In linear gradient elution chromatography, the peak compression factor assumes that a) linear solvent strength (LSS) model applies to the retention of the sample, b) the efficiency of the column is independent of the mobile phase composition, and c) the relative retention factor of a compound inside its band varies linearly with the distance from the band center (see e.g. Gritti and Guiochon (2008)).

Assume a gradient elution in the column and that modifier moves through the column bed as an ideal and undistorted wave. The standard deviation of the component peak in time units is given as (e.g. Carta and Stringfield (1992); Gritti and Guiochon (2008); Guiochon et al. (2006))

$$\sigma = C\frac{L_{\max}/u}{\sqrt{N}}\left[1+\frac{Fk_H(\phi_0)}{Fk_H(\phi_0)\alpha\beta+1}\right], \tag{43}$$

where $\beta = (\phi_e - \phi_0)/(\eta_e - \eta_s)$. Here, N denotes the plate number and C is a band or peak

compression factor, which are defined as

$$N = \frac{\left(\mu_{1,\mathrm{iso}} - \frac{t_{\mathrm{inj}}}{2}\right)^2}{\mu'_{2,\mathrm{iso}} - \frac{t_{\mathrm{inj}}^2}{12}}, \quad C = \frac{\sqrt{1+p+p^2/3}}{1+p}, \tag{44}$$

where $\mu_{1,\mathrm{iso}}$ and $\mu'_{2,\mathrm{iso}}$ are given by Eqs. (40) and (41), while

$$p = -\frac{Fk_H(\phi_0)\alpha\beta}{1+Fk_H(\phi_0)}. \tag{45}$$

C represents the ratio of the standard deviation obtained in gradient elution and the standard deviation obtained if the peak were eluted isocratically at the modulator concentration at which the peak elutes in the gradient. C is less than one.

Using the second cental moment in Eq. (37), the standard deviation σ for a gradient considering infinitesimal feed pulse is calculated as

$$\sigma = \sqrt{\mu'_2 - \frac{t_{\mathrm{inj}}^2}{12}}. \tag{46}$$

Figure 7 compares the values of σ calculated from Eq. (43) with those calculated from Eq. (46) as a function of the slope $\beta/t_0 = (\phi_e - \phi_0)/(t_e - t_s)$. Here, $t_s = 5$ min, $t_e = 80$ min and $\phi_0 = 0.1$ were kept fixed, while ϕ_e was changed to get different values of β/t_0. All other parameters are taken from Table 1. A good agreement can be seen between the standard deviation calculated from our moments expressions (c.f. Eq. (46)) and the one obtained by Eq. (43) for small feed pulses. A similar agreement between the two expressions can, of course, be expected for C.

Figure 8 compares the gradient and isocratic two-component elutions. In Figure 8(a) the outlet profiles of both components are plotted for isocratic and gradient elutions. Here, we have chosen a case in which rather two large retention factors differ significantly, which

represents a situation in which typically gradients are applied. The following values were used: $k_{H_r,1} = 10$, $k_{H_r,2} = 30$, $\phi_e = 0.95$, $\alpha = 0.95$, $t_s = 1$ min, $t_e = 280$ min, and other parameters are taken from Table 1. Due to pronounced difference in the retention factors of the components, a wide gap is present between the two peaks during isocratic elution. This gap affects the cycle time and, thus, productivities is considerably altered in gradient elution. For illustration, Figure 8(b) shows the elution profiles for the same gradient starting time but different gradient steepness which are generated by changing the gradient end time t_e. The plots show that steeper gradients (i.e. earlier end times) reduce the distance between the peaks and the cycle time and, thus, enhances productivity. The plots show that gradient steepness has significantly influenced the retention of more retained component 2. The solutions derived in this paper provide a suitable tool to optimize gradient start and end times and the starting and ending levels of the solvent strength.

7. Conclusions

The transport model was used to derive analytical solutions and temporal moments of the response peak in linear gradient elution chromatography. For this a coordinate transformation was used together with the Laplace transform approach. The Laplace domain solution was used to derive up to now unknown analytical moment expressions in the transformed and actual time domains. Compared to isocratic elution, the derivation of analytical solutions and moments for gradient elution is more complicated, because the retention behavior of the solute in this operation mode varies with a change in the mobile-phase composition.

Several case studies were conducted. The effects of starting and ending times of gradient, magnitude of modulator concentration, solvent strength, gradient slope, and mass transfer coefficient were analyzed on the elution profiles and moments. The advantages of gradient elution over isocratic elution were demonstrated and its potential application to analytical chromatography was explored. The results of this research work can be useful for solving parameter estimation (inverse) problems and for analyzing and optimizing the analytical and preparative liquid chromatography exploiting gradient elution. It should be noted that although application examples were presented for cases where the interaction strength decrease as the modulator concentration increases ($\alpha > 0$), thereby requiring a positive gradient, the same relationships apply when ($\alpha < 0$) and the interaction strength increases with the modulator concentration, thereby requiring a negative gradient. In practice, the former case is found in reverse phase chromatograph (RPC), where ϕ is the volume fraction of an organic modifier. The latter case is found in hydrophobic interaction chromatography (HIC), where ϕ is the concentration of a kosmotropic salt such as ammonium sulfate.

Appendix A

A. Analytical moments in the $(\boldsymbol{\eta}, \boldsymbol{\xi})$ coordinates

Now, we use now Eq. (29) to derive analytical expressions of temporal moments $\tilde{\mu}_n$ and central temporal moments $\tilde{\mu}'_n\,(n \geq 2)$ at the column outlet. Lets define (c.f. Eq. (12))

$$\xi_R = \eta_R - 1, \tag{A-1}$$

where

$$\eta_R = t_R/t_0, \tag{A-2}$$

denotes a dimensionless retention time with t_R being the usual retention time for gradient elution (or the first temporal moment). The following well-known relationship, rigourously derived by Nikitas and Pappa-Louisi (2005), can be used to predict this dimensionless retention time in gradient elution, which also comes out from Eq. (32) for $x = 1$ and $s = 0$:

$$\int_0^{\xi_R} \frac{1}{Fk_H(\theta)} d\theta = 1. \tag{A-3}$$

The above equation is utilized to find the value of unknown $\xi_R := f(0,1)$ (c.f. Eq. (32)). By using Eqs. (30) and (A-3) the value of ξ_R is obtained as

$$\xi_R = \begin{cases} Fk_H(\phi_0), \quad \text{for } 0 \le \xi_0 < \eta_s, \\ \eta_s + \frac{1}{\alpha\beta} \ln\left[1 + \alpha\beta\left(Fk_H(\phi_0) - \eta_s\right)\right], \quad \text{for } \eta_s \le \xi_0 \le \eta_e, \\ \eta_e + Fk_H(\phi_e) - \eta_s \frac{Fk_H(\phi_e)}{Fk_H(\phi_0)} - \frac{[\exp(\alpha\beta(\eta_e - \eta_s)) - 1]}{\alpha\beta} \frac{Fk_H(\phi_e)}{Fk_H(\phi_0)}, \text{ for } \xi_0 > \eta_e, \end{cases} \tag{A-4}$$

where $\xi_0 = Fk_H(\phi_0)$.

On replacing ξ by ξ_R in Eq. (29) and using the following well-known moment generating formulas (see Vander (1958)), we can calculate the first three moments of the response peak.

The zeroth moment is given as

$$\tilde{\mu}_0(\xi_R) = \lim_{s \to 0} \bar{c}(s, \xi_R). \tag{A-5}$$

While, the normalized nth moment is obtained as

$$\tilde{\mu}_n(\xi_R) = \frac{(-1)^n}{\tilde{\mu}_0(\xi_R)} \lim_{s \to 0} \frac{d^n \bar{c}(s, \xi_R)}{ds^n}, \text{ for } n = 1, 2, \cdots. \tag{A-6}$$

By utilizing Eqs. (29) and (A-5), the zeroth moment is given as

$$\tilde{\mu}_0(\xi_R) = \frac{Fk_H(\phi_0)}{Fk_H(\xi_R)} c_{\text{inj}} \eta_{\text{inj}}. \tag{A-7}$$

By using Eqs. (29) and (A-6) (for $n = 1$), the normalized first moment is found to be:

$$\tilde{\mu}_1(\xi_R) = \frac{\eta_{\text{inj}}}{2} + 1 + \xi_R - \frac{1}{\kappa_m}\left[\frac{1}{Fk_H(\phi_0)} - \frac{1}{Fk_H(\xi_R)}\right]. \tag{A-8}$$

In the above equation, the third and fourth terms, which contain the gradient dependent Henry constant, decide for a decrease or an increase in the retention time during the gradient elution. For a positive value of the modulator concentration ($\alpha > 0$) or slope ($\beta > 0$), which gives a positive gradient, the interaction strength decreases and, hence, the retention time decreases. On the other hand, a negative value of the modulator concentration ($\alpha < 0$) or slope ($\beta < 0$) provides a negative gradient that increases interaction strengths, thereby giving a larger retention time. Under typical conditions the third term has a strong impact on the value of $\tilde{\mu}_1$, while the effect of last (fourth) term has is negligible.

Similarly, the normalized second moment can be expressed as

$$\begin{aligned}\tilde{\mu}_2(\xi_R) =& \frac{\eta_{\text{inj}}^2}{3} + \eta_{\text{inj}}\left(1 + \xi_R - \frac{1}{\kappa_m}\left[\frac{1}{Fk_H(\phi_0)} - \frac{1}{Fk_H(\xi_R)}\right]\right) - \frac{2(1+\xi_R)}{\kappa_m}\left[\frac{1}{Fk_H(\phi_0)} - \frac{1}{Fk_H(\xi_R)}\right] \\ &+ (1+\xi_R)^2 - \frac{2}{\kappa_m^2}\left[\frac{1}{F^2 k_H(\xi_R) k_H(\phi_0)} - \frac{1}{F^2 k_H^2(\xi)}\right] + 2\int_0^{\xi_R} \frac{1}{F^2 k_H^2(\theta)\kappa_m} d\theta. \end{aligned} \tag{A-9}$$

By using Eqs. (A-8) and (A-9), the normalized central moment is calculated as

$$\begin{aligned}\tilde{\mu}_2'(\xi_R) &= \tilde{\mu}_2(\xi_R) - (\tilde{\mu}_1(\xi_R))^2 \\ &= \frac{\eta_{\text{inj}}^2}{12} + 2\int_0^{\xi_R} \frac{1}{F^2 k_H^2(\theta)\kappa_m} d\theta - \frac{1}{\kappa_m^2}\left[\frac{1}{F^2 {k_H}^2(\phi_0)} - \frac{1}{F^2 k_H^2(\xi_R)}\right]. \end{aligned} \tag{A-10}$$

The normalized third moment is expressed as

$$\begin{aligned}\tilde{\mu}_3(\xi_R) =& \frac{\eta_{\text{inj}}^3}{4} + \eta_{\text{inj}}^2\,(1+\xi_R) + \frac{3\eta_{\text{inj}}}{2}\,(1+\xi_R)^2 + (1+\xi_R)^3 - 3\eta_{\text{inj}}\,(1+\xi_R)\,\frac{1}{\kappa_m}\left[\frac{1}{Fk_H(\phi_0)} - \frac{1}{Fk_H(\xi_R)}\right] \\ & - 3\,(1+\xi_R)^2\,\frac{1}{\kappa_m}\left[\frac{1}{Fk_H(\phi_0)} - \frac{1}{Fk_H(\xi_R)}\right] - \eta_{\text{inj}}^2\frac{1}{\kappa_m}\left[\frac{1}{Fk_H(\phi_0)} - \frac{1}{Fk_H(\xi_R)}\right] \\ & - 3\eta_{\text{inj}}\frac{1}{\kappa_m^2}\left[\frac{1}{F^2k_H(\xi_R)k_H(\phi_0)} - \frac{1}{F^2k_H^2(\xi_R)}\right] - 6\,(1+\xi_R)\,\frac{1}{\kappa_m^2}\left[\frac{1}{F^2k_H(\xi_R)k_H(\phi_0)} - \frac{1}{F^2k_H^2(\xi_R)}\right] \\ & + 3\eta_{\text{inj}}\int_0^{\xi_R}\frac{1}{F^2k_H^2(\theta)\kappa_m}d\theta + 6\,(1+\xi_R)\int_0^{\xi_R}\frac{1}{F^2k_H^2(\theta)\kappa_m}d\theta \\ & - \frac{6}{\kappa_m}\left[\frac{1}{Fk_H(\phi_0)} - \frac{1}{Fk_H(\xi_R)}\right]\int_0^{\xi_R}\frac{1}{F^2k_H^2(\theta)\kappa_m}d\theta - \frac{6}{\kappa_m^3}\left[\frac{1}{F^2k_H^2(\xi_R)k_H(\phi_0)} - \frac{1}{F^3k_H^3(\xi_R)}\right] \\ & + 6\int_0^{\xi_R}\frac{1}{F^3k_H^3(\theta)\kappa_m^2}d\theta. \end{aligned} \tag{A-11}$$

By using Eqs. (A-8), (A-9) and (A-11), the normalized central moment is calculated as

$$\begin{aligned}\tilde{\mu}_3'(\xi_R) &= \tilde{\mu}_3(\xi_R) - 3\tilde{\mu}_1(\xi_R)\tilde{\mu}_2(\xi_R) + 2\tilde{\mu}_1(\xi_R)^3 \\ &= 6\int_0^{\xi_R}\frac{1}{F^3k_H^3(\theta)\kappa_m^2}d\theta - \frac{2}{\kappa_m^3}\left[\frac{1}{F^3k_H^3(\phi_0)} - \frac{1}{F^3k_H^3(\xi_R)}\right]. \end{aligned} \tag{A-12}$$

Finally, we specify the integral term appearing in the expressions for the moments. For the given $F^nk_H^n(\theta) = F^nk_H^n(\phi_0)\exp(-n\alpha\beta\theta)$ $(n = 2, 3)$ holds

$$\int_0^{\xi_R}\frac{1}{F^nk_H^n(\theta)}d\theta = \begin{cases} \frac{1}{F^nk_H^n(\phi_0)}\xi_R, & \text{for } 0 \le \xi_R < \eta_s, \\ \frac{1}{F^nk_H^n(\phi_0)}\eta_s + \frac{\exp[n\alpha\beta(\xi_R-\eta_s)]-1}{n\alpha\beta F^nk_H^n(\phi_0)}, & \text{for } \eta_s \le \xi_R \le \eta_e, \\ \frac{1}{F^nk_H^n(\phi_0)}\eta_s + \frac{\exp[n\alpha\beta(\eta_e-\eta_s)]-1}{n\alpha\beta F^nk_H^n(\phi_0)} + \frac{1}{F^nk_H^n(\phi_e)}(\xi_R-\eta_e), & \text{for } \xi_R > \eta_e. \end{cases} \tag{A-13}$$

Once again, the second and third terms in $\tilde{\mu}_2'(\xi_R)$ and $\tilde{\mu}_3'(\xi_R)$, which contain the gradient dependent Henry constant, decide about a possible decrease or increase in the variance and asymmetry of profiles during gradient elution (for more details, see the paragraph below Eq. (A-8)).

B. Analytical moments in the (η, x) coordinates

Now, the dimensionless temporal moments in (η, ξ) coordinates are used to obtain the dimensionless temporal moments in the (η, x) coordinates. The dimensionless temporal moments $\mu_{0,d}$, $\mu_{1,d}$ and $\mu'_{2,d}$, and $\mu'_{3,d}$ at the column outlet ($x = 1$) as functions of dimensionless time (η) are given below.

First, using Eq. (A-7), the dimensionless total mass solute at the column outlet is obtained as

$$\mu_{0,d} = \frac{Fk_H(\xi_R)}{Fk_H(\phi_0)}\tilde{\mu}_0 = c_{\text{inj}}\eta_{\text{inj}}. \tag{A-14}$$

The dimensionless mean retention time is obtained from Eq. (A-8) is given as

$$\mu_{1,d} = \frac{\eta_{\text{inj}}}{2} + (1 + \xi_R) - \frac{1}{\kappa_m}\left[\frac{1}{Fk_H(\phi_0)} - \frac{1}{Fk_H(\xi_R)}\right]. \tag{A-15}$$

According to the definition of ξ_R (c.f. Eq. (A-1)):

$$\xi_R = \eta_R - 1. \tag{A-16}$$

Therefore, Eq. (A-15) takes the form:

$$\mu_{1,d} = \frac{\eta_{\text{inj}}}{2} + \eta_R - \frac{1}{\kappa_m}\left[\frac{1}{Fk_H(\phi_0)} - \frac{1}{Fk_H(\xi_R)}\right]. \tag{A-17}$$

The second central moment (c.f. Eq. (A-10)) is obtained as

$$\begin{aligned}\mu'_{2,d} &= \frac{\eta_{\text{inj}}^2}{12} + (\tilde{\mu}'_2(\xi_R) - \frac{\eta_{\text{inj}}^2}{12})F^2k_H^2(\tilde{\xi}_R), \quad \text{for } \tilde{\xi}_R \in (\xi_R, \xi_0) \\ &= \frac{\eta_{\text{inj}}^2}{12} + \frac{2F^2k_H^2(\tilde{\xi}_R)}{\kappa_m}\int_0^{\xi_R}\frac{1}{F^2k_H^2(\theta)}d\theta - \frac{1}{\kappa_m^2}\left[\frac{F^2k_H^2(\tilde{\xi}_R)}{F^2{k_H}^2(\phi_0)} - \frac{F^2k_H^2(\tilde{\xi}_R)}{F^2k_H^2(\xi_R)}\right].\end{aligned} \tag{A-18}$$

Similarly, the third central moment (c.f. Eq. (A-12)) is obtained as

$$\begin{aligned}\mu'_{3,d} &= F^3 k_H^3(\tilde{\xi}_R)\tilde{\mu}'_3(\tilde{\xi}_R) \\ &= \frac{6F^3 k_H^3(\tilde{\xi}_R)}{k_m^2}\int_0^{\xi_R}\frac{1}{F^3\kappa_H^3(\theta)}d\theta - \frac{2}{\kappa_m^3}\left[\frac{F^3 k_H^3(\tilde{\xi}_R)}{F^3 k_H^3(\phi_0)} - \frac{F^3 k_H^3(\tilde{\xi}_R)}{F^3 k_H^3(\xi_R)}\right].\end{aligned} \tag{A-19}$$

References

Baeza-Baeza, J. J., Ortiz-Bolsico, C., Torres-Lapasió, J. R., García-Álvarez-Coque, M. C., 2013. Approaches to model the retention and peak profile in linear gradient reversed-phase liquid chromatography. Chromatogr. A 1284, 28-35.

Carta, G., Stringfield, B. W., 1992. Analytic solution for volume-overloaded gradient elution chromatography. J. Chromatogr. 605, 151-159.

Creasy, A., Lomino, J., Barker, G., Khetan, A., Carta, G., 2018. Gradient elution behavior of proteins in hydrophobic interaction chromatography with U-shaped retention factor curves. J. Chromatogr. A 1547, 53-6.

Donaldson, K. O., Tulane,V. J., Marshall, L.M., 1952. Automatically increasing solvent polarity in chromatography. Anal. Chem. 24, 185-187.

Durbin, F., 1974. Numerical inversion of Laplace transforms: An efficient improvement to Dubner and Abate's method. Comput. J. 17, 371-376.

Gritti, F., Guiochon, G., 2008. Exact peak compression factor in linear gradient elution I. Theory. J. Chromatogr. A 1212, 35-40.

Guan-Sajonz, H., Sajonz, P., Zhong, G., Guiochon, G., 1996. Study of the mass transfer kinetics of BSA on a TSK-GEL DEAE-5PW anion exchanger in a wide concentration range. Biotechnol. Prog. 12, 380-386.

Guiochon, G., 2002. Preparative liquid chromatography. J. Chromatogr. A 965, 129-161.

Guiochon, G., Felinger, A., Shirazi, D.G., Katti, A.M., 2006. Fundamentals of preparative and nonlinear chromatography, 2nd ed. ELsevier Academic press, New York.

Hagdahl, L., Williams, R. J. P., Tiselius, A., 1952. Elution and displacement analysis procedures with special reference to chromatography on carbon. Arkiv Kemi 4, 193-219.

Hao, W., Zhang, X., Hou, K., 2006. Analytical solutions of the ideal model for gradient liquid chromatography. Anal. Chem. 78, 7828-7840.

Hao, W., Di, B., Chen, Q., Wang, J., Yang, Y., Sun, X., 2013. Study of the peak variance in isocratic and gradient liquid chromatography using the transport model. Chromatogr. A 1295, 67-81.

Jandera, P., Churácek, J, 1985. Gradient elution in column liquid chromatography. Elsevier, Amsterdam.

Jandera, P., 2005. Gradient elution in liquid column chromatography-prediction of retention and optimization of separation. Adv. Chromatogr. 43, 1-108.

Jandera, P., 2006. Can the theory of gradient liquid chromatography be useful in solving practical problems? J. Chromatogr. 1126, 195-219.

Javeed, S., Qamar, S., Seidel-Morgenstern, A., Warnecke, G., 2011. Efficient and accurate numerical simulation of nonlinear chromatographic processes. J. Comput. Chem. Eng. 35 (2011) 2294-2305.

Javeed, S., Qamar, S., Ashraf, W., Warnecke, G., Seidel-Morgenstern, A, 2013. Analysis and numerical investigation of two dynamic models for liquid chromatography. Chem. Eng. Sci. 90, 17-31.

Kucera, E., 1965. Contribution to the theory of chromatography: Linear non-equilibrium elution chromatography. J. Chromatogr. A 19, 237-248.

Miyabe, K., Guiochon, G., 2000. Determination of the lumped mass transfer rate coefficient by frontal analysis. J. Chromatogr. A 890, 211-223.

Miyabe, K., 2007. Surface diffusion in reversed-phase liquid chromatography using silica gel stationary phases of different C1 and C18 ligand densities. J. Chromatogr. A 1167, 161-170.

Miyabe, K., 2009. Moment analysis of chromatographic behavior in reversed-phase liquid chromatography. J. Separat. sci. 32, 757-770.

Nicoud, R.-M. 2015. Chromatographic Processes: Modeling, simulation, and design. Cambridge University Press, London.

Nikitas, P., Pappa-Louisi. A., 2005. Expressions of the fundamental equation of gradient elution and a numerical solution of these equations under any gradient profile. Anal. Chem. 77, 5670-5677.

Schneider, P., Smith, J. M., 1968. Adsorption rate constants from chromatography. AIChE J. 14, 762-771.

Ståhlberg, J., 2010. The thermodynamic limit of linear gradient chromatography. Chromatogr. A 1217, 3172-3179.

Suzuki, M., 1973. Notes on determining the moments of the impulse response of the basic transformed equations. J. Chem. Eng. Japan 6, 540-543.

Snyder, L.R., 1986. High performance liquid chromatography-advances and erspectives, in: Cs. Horváth (Ed.), Vol. 1, Wiley, New York, N.Y.

Snyder, L. R., Dolan J. W., 1998. The linear-solvent-strength model of gradient elution. Adv. Chromatogr. N.Y. 38, 115-187.

Snyder, L. R., Dolan, J. W., 2006. High-performance gradient elution: The practical application of the linear-solvent-strength model. Wiley, Hoboken, New Jersey.

Van der Laan, Th., 1958. Letter to the editors on notes on the diffusion type model for the longitudinal mixing in flow. Chem. Eng. Sci. 7, 187-191.

Table 1: Reference parameters used in the simulations.

Parameters	Values
Length of column	$L = 10\,\mathrm{cm}$
Porosity	$\epsilon = 0.4$
Interstitial velocity	$u = 1.0\,\mathrm{cm/min}$
Retention time of non-retained component	$t_0 = 10$ min
Reference Henry's constant	$k_{H_r} = 5$
Solvent strength parameter	$\alpha = 0.8$
Mass transfer coefficient	$k_m = 10\ \mathrm{min}^{-1}$
Injected concentration	$c_{\mathrm{inj}} = 1\,\mathrm{mmol/l}$
Time of injection	$t_{\mathrm{inj}} = 2$ min
Initial concentration of the modulator	$\phi_0 = 0.1$
Final concentration of the modulator	$\phi_e = 0.6$
Gradient start time	$t_s = 5$ min
Gradient end time	$t_e = 80$ min

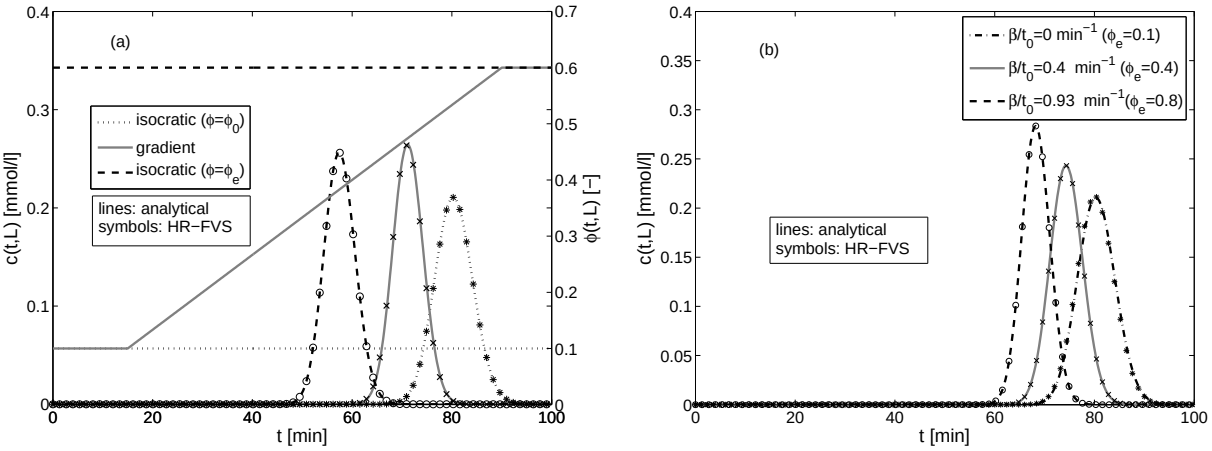

Figure 1: Plot (a) gives a comparison of gradient and isocratic elutions for parameters listed in Table 1. For isocratic elution with $\phi = \phi_0$: $\mu_1 = 80.1$ min, $\mu_2' = 14.2$ min^2 and $\mu_3' = 4.2$ min^3. For gradient elution: $\mu_1 = 71.24$ min, $\mu_2' = 9.1$ min^2 and $\mu_3' = 2.32$ min^3. While, for isocratic elution with $\phi = \phi_e$: $\mu_1 = 57.45$ min, $\mu_2' = 9.64$ min^2 and $\mu_3' = 2.79$ min^3. Plot (b) gives the elution profiles for different values of ϕ_e (or β/t_0), while all other parameters are taken from Table 1.

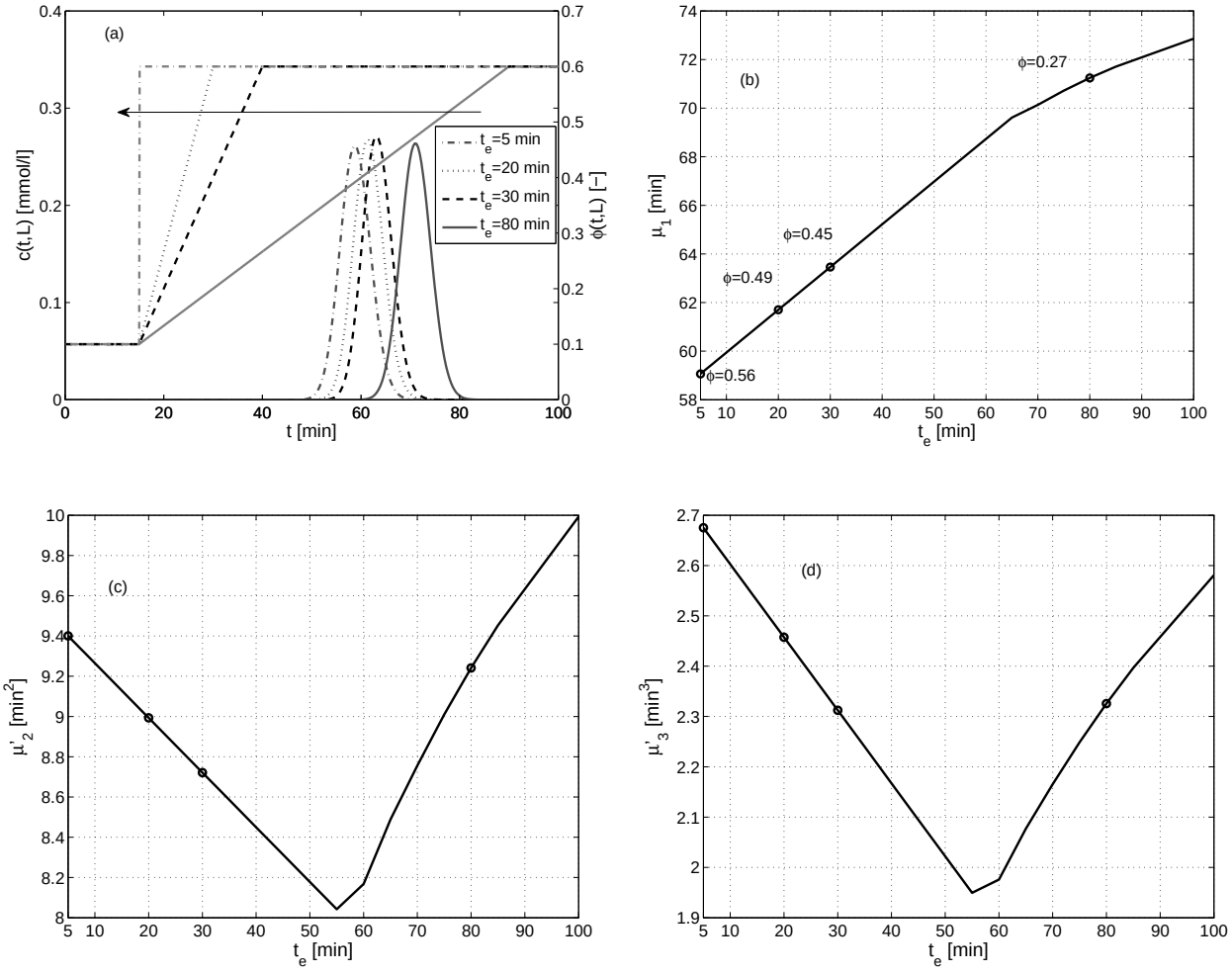

Figure 2: Effect of gradient end time (t_e) on the elution profiles and moments. Here, t_e was changed gradually while all other parameters are taken from Table 1. The marked values of the moments, obtained by numerically integrating the elution profiles, are in good agreement with those calculated directly from the moment expressions.

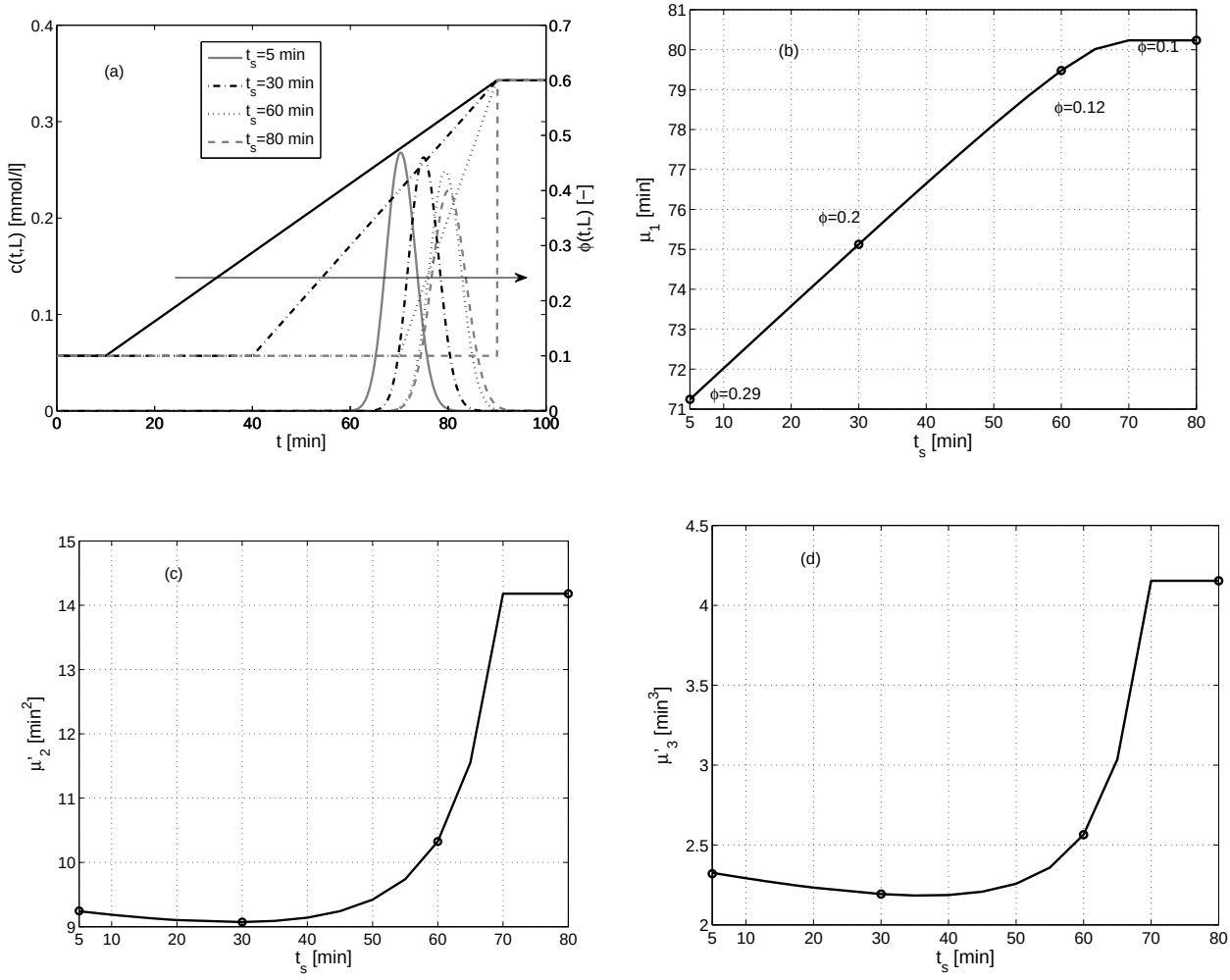

Figure 3: Effect of gradient start time (t_s) on the elution profile and moments. Here, t_s was changed gradually while all other parameters are taken from Table 1. The marked values of moments, obtained by numerically integrating the elution profiles, are in good agreement with those calculated directly from the moment expressions.

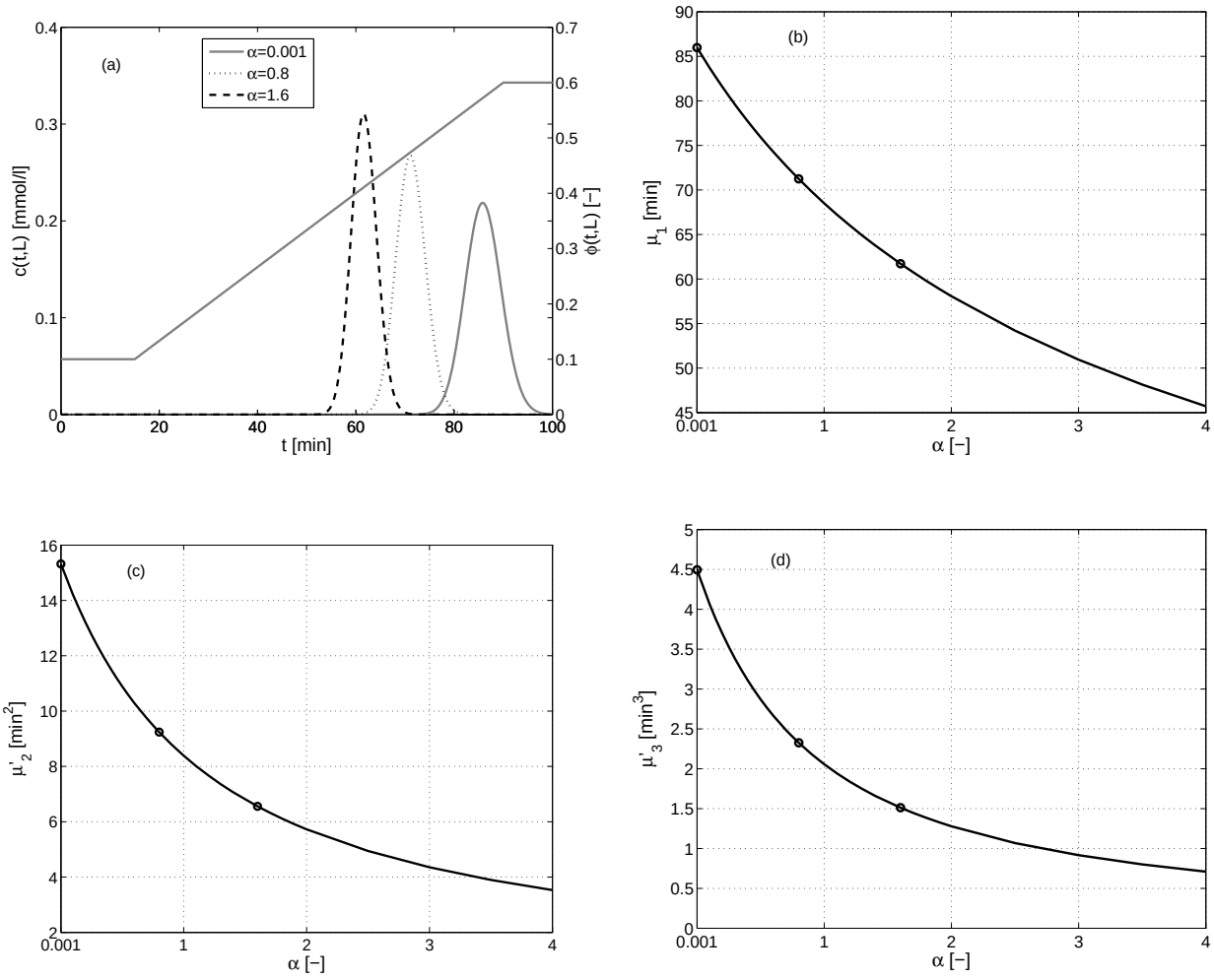

Figure 4: Effect of α on the concentration profiles and moments. Here, α was changed gradually while all other parameters are taken from Table 1. The marked values of the moments, obtained by numerically integrating the elution profiles, are in good agreement with those calculated directly from the moment expressions.

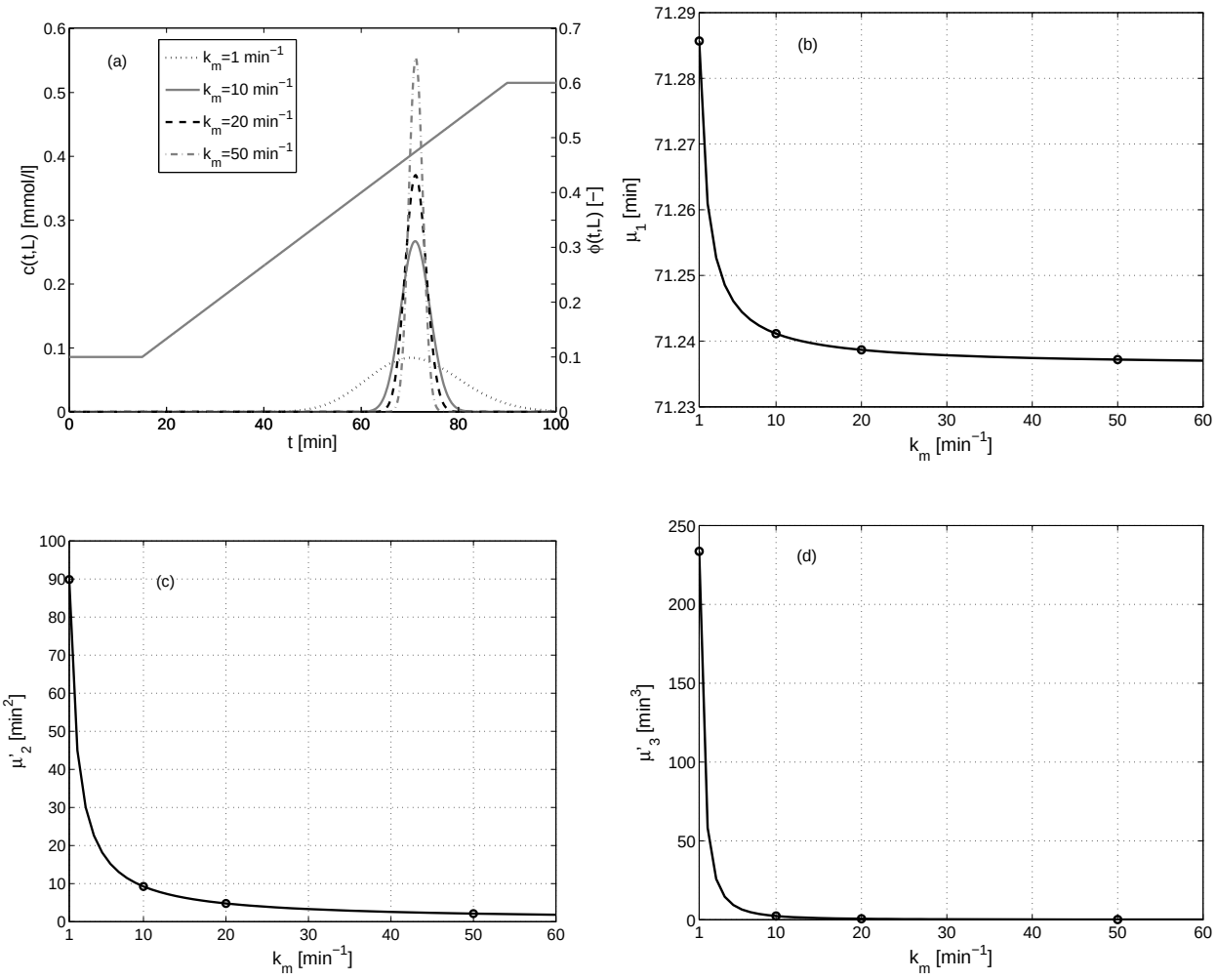

Figure 5: Effect of k_m on the gradient elution. Here, k_m was changed while all other parameters are taken from Table 1. The marked values of the moments, obtained by numerically integrating the elution profiles, are in good agreement with those calculated directly from the moment expressions.

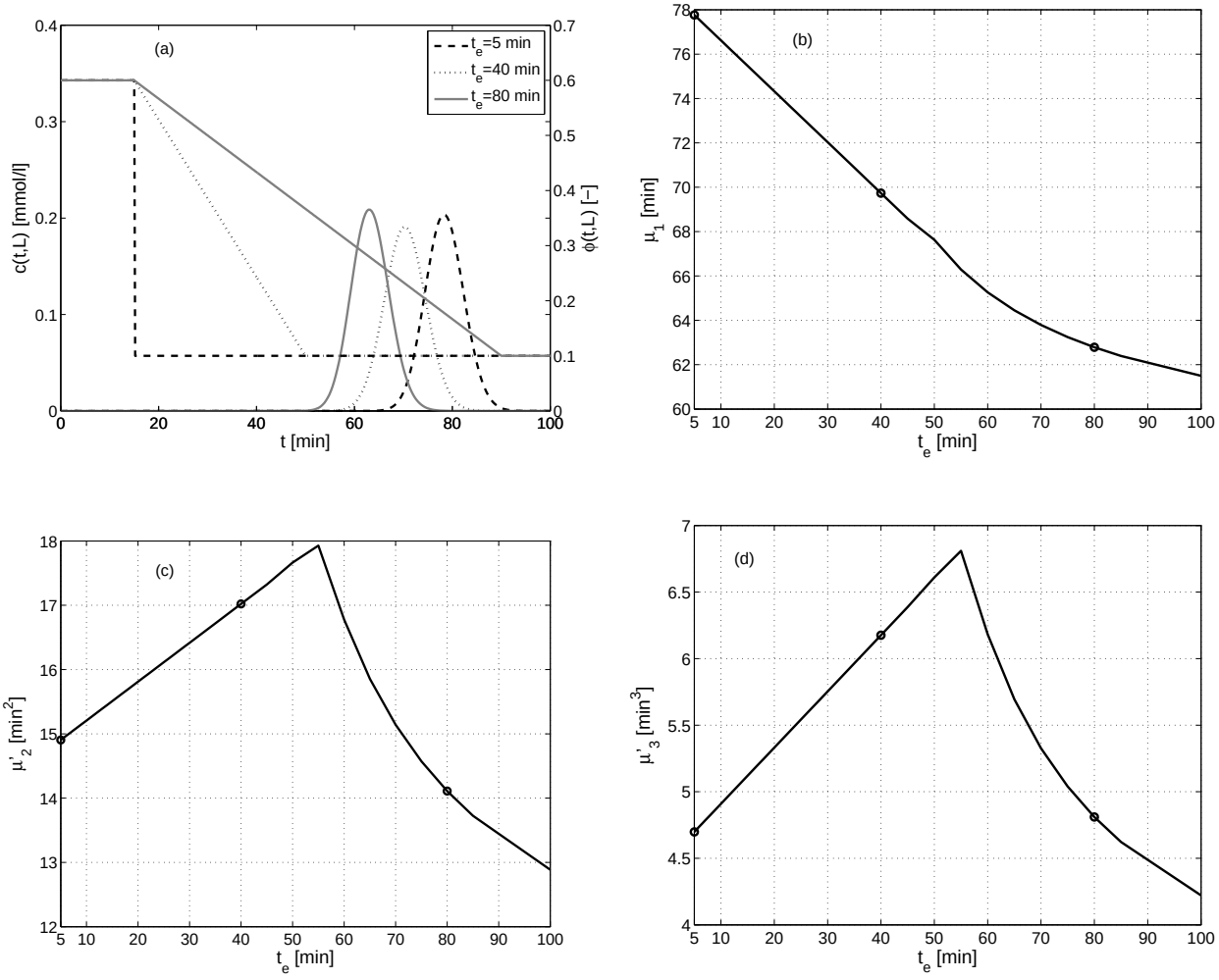

Figure 6: The effect of gradient ending time (t_e) for the case of negative gradient (i.e. $\phi_e < \phi_0$) on the elution profiles and moments. Here, $t_s = 5$ min, $\phi_0 = 0.6$, and $\phi_e = 0.1$. The marked values of the moments, obtained by numerically integrating the elution profiles, are in good agreement with those calculated directly from the moment expressions.

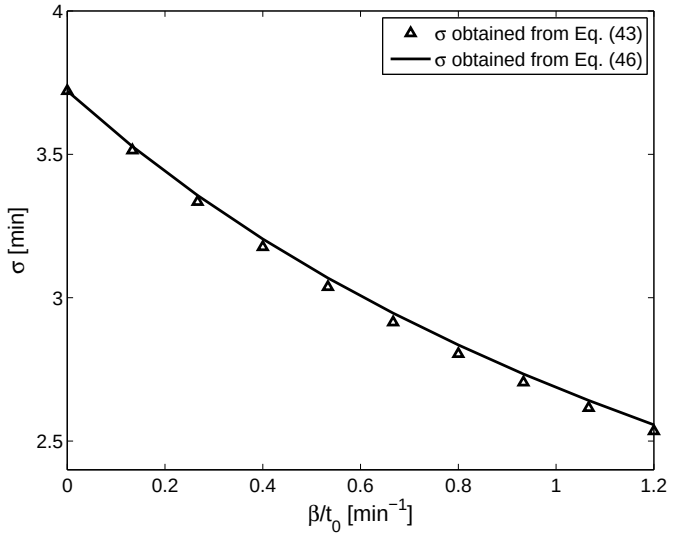

Figure 7: A comparison of the values of σ calculated from Eq. (43) with those calculated from Eq. (46) as a function of the slope $\beta/t_0 = (\phi_e - \phi_0)/(t_e - t_s)$. Here, $t_s = 5$ min, $t_e = 80$ min and $\phi_0 = 0.1$ were kept fixed, while ϕ_e was changed to get different values of β/t_0. All other parameters are taken from Table 1.

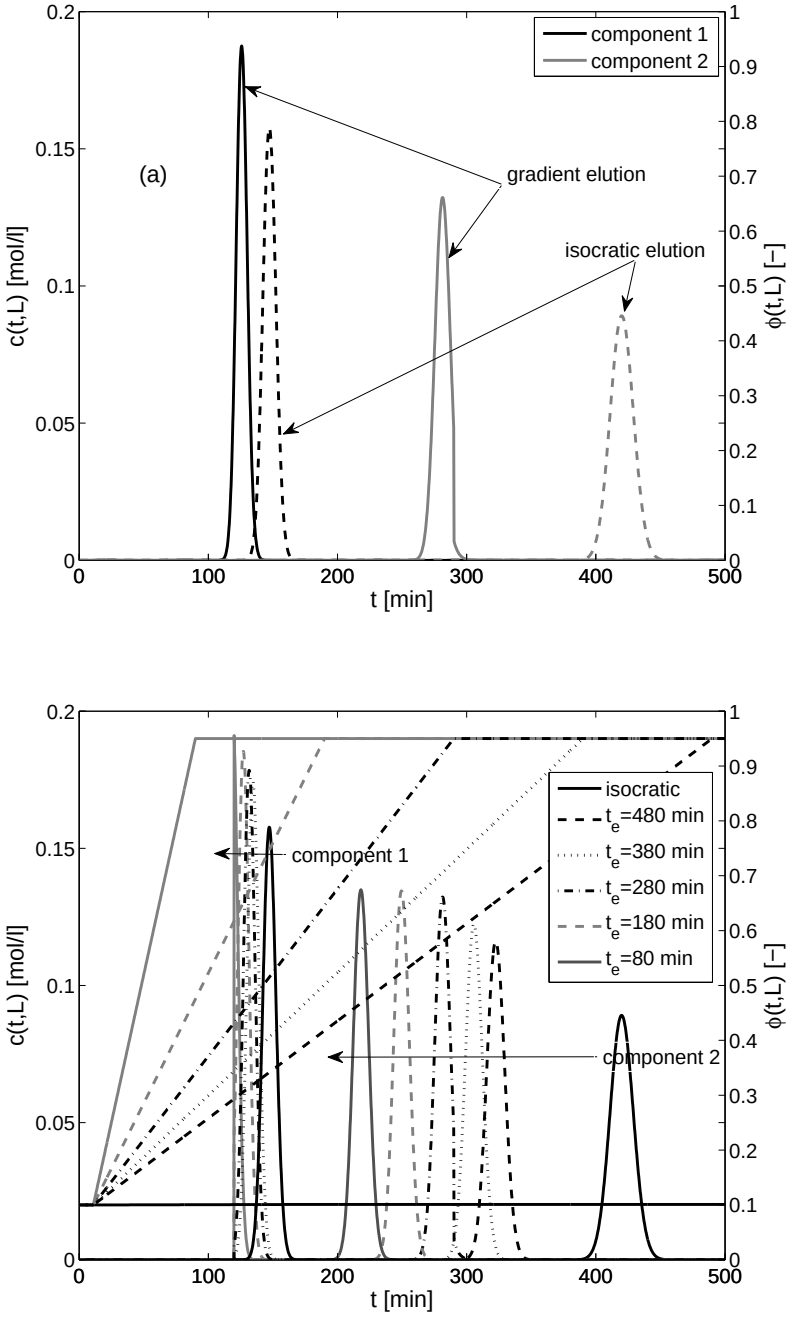

Figure 8: Plot (a) compares gradient and isocratic two-component elutions. Here, we used $k_{H_r,1} = 10$, $k_{H_r,2} = 30$, $\phi_e = 0.95$, $\alpha = 0.95$, $t_s = 1$ min, $t_e = 280$ min, while other parameters are taken from Table 1. Plot (b) shows the elution profiles for different steepness of the gradient obtained by varying the end time t_e.